Joint Power and Location Design for Energy-Efficient Covert UAV Communications

Yangfan Xu, Bin Yang, Yulong Shen, Zhiquan Liu, Xiaohong Jiang, Tarik Taleb

***Abstract*—Unmanned aerial vehicles (UAVs) have been extensively deployed in wireless communication scenario. However, UAV communication faces the challenges of information leakage and energy limitation. Therefore, this paper studies energy-efficient covert communication in adversarial UAV-enabled wireless systems, where a UAV covertly delivers information to a legitimate ground receiver under the detection of a malicious detector with noise uncertainty. Our objective is to maximize covert energy efficiency, defined as the achievable covert throughput per unit of energy consumption, via the joint design of transmit power and flying location. To this end, we derive the detector's minimum detection error probability to establish a covertness constraint. Based on this model, we formulate a three-dimensional joint optimization problem for transmit power and two-dimensional location, capturing the fundamental tradeoff among covertness, communication reliability, and energy efficiency. Through system geometric exploration, metric monotonicity analysis, and theoretical derivation, the original three-dimensional problem is reduced to a one-dimensional search over the flying angle, which enables efficient computation of the optimal UAV configuration via vectorized computation. Numerical results verify the theoretical derivations and illustrate the superiority of the joint design as well as the impact of system parameters on energy efficiency performance.**

***Index Terms*—Physical layer security, covert communication, energy efficiency, UAV systems.**

I. Introduction

Unmanned aerial vehicles (UAVs) have been extensively deployed in diverse wireless communication scenarios such as low-altitude economy, remote sensing and Internet of Things (IoT) [1]–[3]. However, UAV communications, due to the openness of the air-to-ground line-of-sight (LoS) channel, are susceptible to malicious user eavesdropping, facing critical security risks in signal transmission [4]. Traditional signal encryption technique usually requires high computational complexity for UAVs with limited energy [5]. Covert communications are a cutting-edge information security technology that prevents signals from detection by malicious users with the randomness of the wireless channel [6], [7]. Therefore, it is worth investigating how to ensure the covertness of communication processes while increasing the covert throughput per unit of energy (i.e., covert energy efficiency) in energy-limited UAV communication systems.

By now, covert communications have been extensively studied in two main cases: without considering the energy issue and with the energy issue (See the Related Work of Section II in detail). For covert communications without the energy issue, previous works achieved communication covertness through noise uncertainty, channel state uncertainty, and interference uncertainty [8]–[10]. Moreover, some typical techniques that can introduce uncertainty at the detector were considered as solutions for covert communication, such as multiple antennas [11], millimeter wave (mm-Wave) [12], channel inversion power control (CIPC) [13], and reconfigurable intelligent surface (RIS) [14]. Covert communications were also popular to support various applications in diverse scenarios, such as cognitive radio [15], IoT [16], relaying [17], [18] and non-orthogonal multiple access (NOMA) systems [19]. In UAV networks, the previous works [20]–[24] focused on designing the flight trajectory or location of UAVs to further improve the performance of covert communications. For works considering energy issues [25]–[32], the energy-efficient covert communication schemes were designed in energy-limited scenarios such as device-to-device (D2D), backscatter, underwater, UAV, vehicular communications, and integrated sensing and communication (ISAC). These works increased energy efficiency or decreased energy consumption through power control, location selection, beamforming design and resource allocations.

For UAV covert communication scenarios, the energy-limited UAVs are usually deployed to guarantee the quality of service (QoS) of users. Therefore, it is crucial to explore the energy-efficient covert communications in UAV communication systems. A fundamental distinction between UAV and ground communication systems lies in the fact that the flying angles, formed by the UAV's location and the ground nodes, determine the proportion of line-of-sight (LoS) and non-line-of-sight (NLoS) channel components in the air-ground channel.

This work is supported in part by the National Natural Science Foundation of China under Grant 62372076, in part by the Education Department Research Foundation of Anhui Province under Grant DTR2023051, in part by the Innovation Research Team on Future Network Technology of Chuzhou University, in part by the Innovation Team on Smart Home Appliance Security and Applications of Chuzhou City, in part by the Innovative Research Team on Application of Big Data and Financial Technology of Chuzhou University, in part by the Federal Ministry of Research, Technology, and Space (BMFTR), Germany, through the Project 6GEM+ under Grant 16KIS2411, in part by the European Union's Horizon Europe research and innovation programme under the 6G-Path project under Grant 101139172, and in part by the Yunnan Provincial Major Science and Technology Special Program under Grant 202602AC080004. (Corresponding authors: Bin Yang; Yulong Shen).

Yangfan Xu is with the School of Computer and Information Engineering, Chuzhou University, Chuzhou 239000, China and the School of Computer Science and Technology, Anhui University, Hefei 230000, China (e-mail: xuyangfan1112@gmail.com).

Bin Yang is with the School of Computer and Information Engineering, Chuzhou University, Chuzhou 239000, China (e-mail: yangbinchi@gmail.com).

Yulong Shen is with the School of Computer Science and Technology, Xidian University, Xi'an 710071, China (e-mail: ylshen@mail.xidian.edu.cn).

Zhiquan Liu is with the College of Cyber Security, Jinan University, Guangzhou 510632, China (e-mail: zqliu@jnu.edu.cn).

Xiaohong Jiang is with the School of Systems Information Science, Future University Hakodate, Hakodate 041-8655, Japan (e-mail: jiang@fun.ac.jp).

Tarik Taleb is with the Faculty of Electrical Engineering and Information Technology, Ruhr University Bochum, Bochum 44801, Germany (e-mail: tarik.taleb@rub.de).

TABLE I
DIFFERENCES BETWEEN OUR WORK AND OTHER RELATED WORKS

References	UAV Communication	Covert Energy Efficiency	Joint Power and Location Design	Flying Angle Analysis	LoS/NLoS Channel Model	Noise Uncertainty	Throughput Requirement	Low-complexity Design
[20]	✓	×	×	×	×	×	×	✓
[21]	✓	×	✓	✓	✓	×	×	✓
[22]	✓	×	×	×	×	×	×	×
[23]	✓	×	×	×	×	×	×	×
[24]	✓	×	✓	×	×	✓	✓	×
[25]	×	✓	×	×	×	×	×	×
[26]	×	×	×	×	×	×	×	×
[27]	×	×	×	×	×	✓	×	✓
[28]	×	×	×	×	×	×	×	×
[29]	×	✓	×	×	×	×	×	×
[30]	×	✓	×	×	×	×	×	×
[31]	✓	×	×	×	×	×	✓	✓
[32]	✓	✓	✓	×	×	✓	×	×
Our Work	✓	✓	✓	✓	✓	✓	✓	✓

Specifically, a larger flying angle increases the LoS probability and enhances the received signal, while a smaller flying angle promotes the NLoS component with significantly higher path loss. However, there are only a few works on the UAV covert communications with energy issue, for example [31] and [32], which model the air-ground channels as purely LoS channels, ignoring the proportion of NLoS component in the air-ground channel. Furthermore, these studies ignore the impact of flying angles on system performance for optimal location design.

In UAV communication systems, this angle-dependent LoS/NLoS mechanism has a critical impact on covert communication. The flying angle relative to the detector controls the strength of signal leakage, thereby affecting covertness, while the flying angle relative to the receiver determines the channel quality, consequently impacting throughput. Since these two angles are geometrically coupled via the single UAV's location, adjusting the location to enhance covertness unavoidably impacts throughput, and vice versa. Furthermore, introducing energy efficiency as an optimization objective further couples location-dependent throughput with transmit power. The UAV's transmit power is constrained by covertness requirements, reflected in the power received by the detector, which is also dependent on the UAV's location. Therefore, to explore energy-efficient covert UAV communications, it is necessary to comprehensively consider UAV transmit power, location, flying angle, and realistic LoS/NLoS channel components to more carefully evaluate covertness, throughput, and covert energy efficiency. This coupling resulting from such a comprehensive consideration means that the energy-efficient covert communication problem for the UAV will be a complex joint optimization problem. This problem needs to be solved efficiently for UAV platforms with limited computational resources and rapid deployment requirements.

Motivated by the above analysis, this paper investigates energy-efficient covert UAV communication by jointly optimizing the UAV's transmit power and two-dimensional flying location (including distance and flying angle), while explicitly considering the LoS/NLoS channel model, noise uncertainty and throughput requirement. To address this coupled and complex problem, this paper conducts system geometric exploration, metric monotonicity analysis, and theoretical derivations to transform the problem into a one-dimensional search over flying angle that possesses global optimality. Consequently, the optimal UAV configuration can be efficiently determined through vectorized computation, which is suitable for UAV platforms. To highlight the contributions of our work, the differences between our work and existing works are shown in Table I. The main contributions of this paper can be summarized as follows.

1) In a UAV communication system for surveillance with both LoS and NLoS channel components, we first model covert energy efficiency as the throughput per unit energy, and derive the minimum detection error probability under noise uncertainty. Then, we formulate covert energy efficiency maximization as a joint optimization problem for transmit power and two-dimensional location, subject to the constraints of covertness, throughput, transmit power and flying location.
2) We prove that the optimal distance between the UAV and the detector is the maximum allowable distance, and then derive the maximum covert energy efficiency as a function of the flying angle. The original three-dimensional problem is reduced to a one-dimensional search over the flying angle, which can be efficiently solved via vectorized computation. Furthermore, we derive feasibility conditions for the optimization problem, reflecting the trade-off among the constraints.
3) Numerical results confirm the theoretical derivation and reveal that the proposed joint design has better performance on the maximum covert energy efficiency compared to benchmark schemes. Moreover, we find that the covertness requirement and maximum transmit power primarily determine the feasibility of covert communication, while the minimum throughput requirement governs both feasibility and covert energy efficiency level.

The following sections are organized as follows: The related work is introduced in Section II. System model and communication performance are studied in Section III. Section IV derives the minimum detection error probability. The optimization problem is proposed and solved in Section V. Numerical results are given in Section VI. Section VII concludes this paper.

II. Related Work

A. Covert Communications without Energy Issues

For the covert communications without the energy issue, the works in [8], [9] and [10] introduce noise uncertainty, channel state uncertainty, and interference uncertainty to achieve covertness, respectively. The work in [11] equipped the transmitter and jammer with multiple antennas to improve the covert transmission throughput. The work in [12] found the directional nature of mm-Wave communication contributes to covertness. The work in [13] utilized CIPC to introduce uncertainty by adjusting the transmit power based on the channel coefficient, thus ensuring covert communication performance. The work in [14] adopted RIS to assist covert communications by adjusting phase shifts and reflection amplitude to enhance transmission reliability. Moreover, covert communication was applied in various scenarios. For example, the work in [15] applied covert communications in cognitive radio systems to guarantee both the covertness and spectrum efficiency. The work in [16] maximized covert throughput with power control for D2D communications in IoT systems. The work in [17] proposed a power allocation strategy to ensure simultaneous secure and covert communications in a two-hop relaying system with an untrusted relay. Recently, the work in [18] proposed a dual-function RIS-assisted cooperative relaying communication system with enhanced transmission and backscattering, and explored the reliability, covertness, and security performance of the system. The work in [19] utilized a simultaneously transmitting and reflecting RIS to assist covert communication in NOMA systems, revealing that the proper power allocation can enhance the system's covert throughput.

For covert communications in UAV-assisted systems, the work in [20] provided an artificial potential field approach to maximize the covert throughput by resource allocation and trajectory optimization. The work in [21] maximized covert throughput by optimizing transmit power and flying location of the UAV. The work in [22] proposed a covert communication scheme to counter the UAV detector in a NOMA network where the legitimate UAV can safely receive information from multiple ground users simultaneously. Recently, the work in [23] jointly designed the UAV's beamforming vector and flight trajectory in an ISAC network, aiming to maximize the covert rate under multiple detectors. The work in [24] considered the UAV relaying information while monitoring backscatter communications, aiming to maximize the covert backscatter communication rate under the worst case that the UAV sets the optimal detection threshold, transmit power and hovering location.

B. Covert Communications with Energy Issues

For the covert communications with the energy issue, the work in [25] considered energy-efficient covert D2D communications achieved by transmit probability and power control. The work in [26] proposed an energy-efficient covert offloading scheme in blockchain-enabled IoT systems by optimizing artificial noise power and computation resources. The work in [27] focused on minimizing transmit power in backscatter systems while ensuring both covertness and communication reliability. The work in [28] jointly optimized the trajectory and transmit power of the underwater vehicle, aiming to improve covert throughput and reduce energy consumption for underwater communication. Recently, the work in [29] considered various channel state estimation errors in an ISAC network, achieving energy efficiency maximization through the sensing and information beamforming design. The work in [30] achieved covert vehicular communication, maximizing the covert energy efficiency of vehicle-to-vehicle links and the throughput of vehicle-to-infrastructure links through power control and jamming selection.

For the covert energy issue in UAV communication systems, the work in [31] determined the UAV's optimal hovering altitude and prior transmission probability for covert communication with energy replenishment. The work in [32] modeled a UAV-assisted backscatter system, in which the horizontal coordinate and transmit power of the UAV are jointly optimized to maximize covert energy efficiency under a fixed flight altitude.

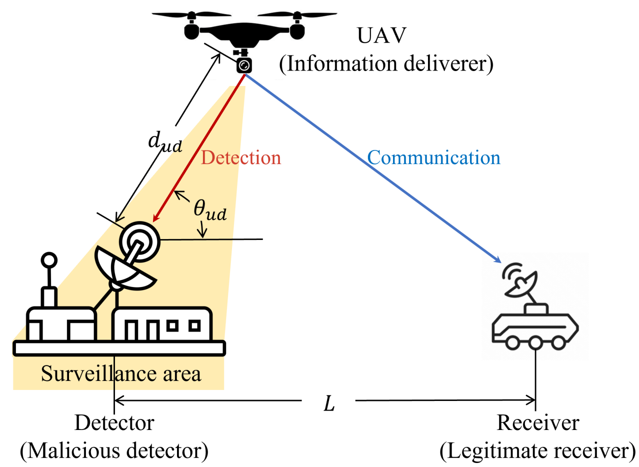

Fig. 1. Illustration of the UAV communication system for surveillance.

III. System Model

As illustrated in Fig. 1, we consider a UAV-enabled wireless system for surveillance consisting of a UAV information deliverer, a ground legitimate receiver (Receiver) and a ground malicious detector (Detector). The UAV acts as both a monitor and a transmitter, aiming to surveil Detector while covertly transmitting confidential information to Receiver without being detected by Detector.

A. Location Model

We assume that the UAV flies within a vertical plane that is perpendicular to the ground and passes through the line connecting Receiver and Detector. This is because this vertical plane is the optimal plane in terms of both communication covertness and throughput. This means that, in three-dimensional space, the optimal azimuth is zero, as proven by previous studies [33], [34]. Specifically, the work in [33] shows that the UAV's location achieving optimal covertness subject to throughput requirements lies on the vertical plane with zero azimuth, and [34] proves that the UAV's location with optimal covert throughput is also on this vertical plane. Due to the fact that the UAV is dispatched by Receiver to perform surveillance on Detector, the UAV has complete knowledge of Receiver's and Detector's locations. The distance between the UAV and Detector is d_{ud}, the distance between Detector and Receiver is L, and the flying angle of the UAV relative to Detector is θ_{ud}.

To avoid visual detection, the UAV needs to maintain a minimum distance from Detector $\underline{d}_{ud}$, while ensuring a good surveillance quality requires a maximum distance $\overline{d}_{ud}$ and a minimum flying angle $\underline{\theta}_{ud}$. Therefore, the UAV's flying location constraints are given by

$$\underline{d}_{ud} \leq d_{ud} \leq \overline{d}_{ud}, \tag{1a}$$

$$\underline{\theta}_{ud} \leq \theta_{ud} \leq \frac{\pi}{2}, \tag{1b}$$

where the constraint $\theta_{ud} \leq \frac{\pi}{2}$ ensures that the UAV stays on the right side of Detector, i.e., the side near Receiver, as shown in Fig. 1. The flying location constraints determine the UAV's feasible flight range. In the practical scenario for UAV surveillance, Receiver is commonly far from Detector, while the deployed UAV performs surveillance above the areas around Detector. This means the UAV is far from Receiver and close to Detector, resulting in a shorter distance between the UAV and Detector than between Receiver and Detector. Thus, L is much larger than d_{ud}, so we consider that $d_{ud} < L$ in this scenario.

B. Channel Model

We consider that each of the UAV, Receiver, and Detector uses one antenna. The channels of UAV-Receiver and UAV-Detector are modeled as air-to-ground wireless channels with LoS and NLoS components [21], [35]. Specifically, the path loss ρ_k of the wireless channel is given by

$$\rho_k = \begin{cases} d_{uk}^{\xi_{\mathrm{L}}}, & \text{for LoS component,} \\ d_{uk}^{\xi_{\mathrm{N}}}, & \text{for NLoS component,} \end{cases} \tag{2}$$

where $k \in \{r, d\}$, d_{uk} denotes the distance from the UAV to Receiver or Detector. The parameters ξ_L and ξ_N correspond to the path loss exponents of the LoS and NLoS channel components, respectively. We also denote the probability of the LoS components in these channels by p_k, which is given by

$$p_k = \frac{1}{1 + a\exp(-180b\theta_{uk}/\pi + ab)}, \tag{3}$$

where a and b represent S-curve parameters relying on the wireless environment, and θ_{uk} ($k \in \{r, d\}$) is the flying angle of the UAV relative to Receiver or Detector.

The UAV-ground receiver/detector link actually consists of both LoS and NLoS channel components. Due to fewer obstructions in the air-ground link, the LoS channel component plays a dominant role compared to the NLoS channel component. In this paper, we consider that the NLoS component is ignored in the UAV-Receiver link, while both LoS and NLoS components are taken into account for the UAV-Detector link. This can be explained as follows. Regarding the system model, the UAV is located far from Receiver, and the NLoS component suffers severe attenuation, making it negligible. In contrast, the UAV hovering closer to Detector means that, for a sensitive detector, the received power from the NLoS component can still affect detection performance. Regarding the system performance, ignoring the NLoS component for the UAV-Receiver link leads to a slightly lower throughput than the throughput with the NLoS component. Conversely, fully retaining the NLoS component for the UAV-Detector link makes Detector receive more leaked signal power and thus have stronger detection capability, compared to ignoring the NLoS component. Satisfying throughput and covertness requirements under this channel modeling ensures that the system achieves better throughput while maintaining strict covertness in real-world deployments.

C. Transmission Performance from UAV to Receiver

In some open outdoor environments with minimal obstructions, we consider that for the channel of UAV-Receiver, the LoS component has a significantly stronger influence than the NLoS component. Therefore, the path gain in the NLoS component is often negligible. Here, we consider a scenario where the UAV sends message $x[i]\,(i = 1, 2, ..., n)$. Let P denote the UAV's transmit power. $\mathcal{H}_0$ indicates that the UAV does not transmit signals, and $\mathcal{H}_1$ indicates the UAV is transmitting. $y_r[i]$ denotes the received signal at Receiver, which is given by

$$y_r[i] = \begin{cases} n_r[i], & \mathcal{H}_0, \\ \sqrt{P d_{ur}^{\xi_L} p_r}\, x[i] + n_r[i], & \mathcal{H}_1, \end{cases} \tag{4}$$

where $n_r[i] \sim \mathcal{CN}(0, \sigma_r^2)$ is the noise received by Receiver. Therefore, the signal-to-noise ratio (SNR) at Receiver γ_r can be expressed as

$$\gamma_r = \frac{P d_{ur}^{\xi_L} p_r}{\sigma_r^2} = \frac{P f(d_{ud}, \theta_{ud})}{\sigma_r^2}, \tag{5}$$

where $f(d_{ud}, \theta_{ud})$ is the function related to d_{ud} and θ_{ud}. $d_{ur}^{\xi_L} p_r$ can be expressed by $f(d_{ud}, \theta_{ud})$ following the geometric positional relationships given in Fig. 1, which is given by

$$\begin{aligned} f(d_{ud}, \theta_{ud}) &= d_{ur}^{\xi_L} p_r \\ &= \frac{\left(L^2 + d_{ud}^2 - 2d_{ud}L\cos(\theta_{ud})\right)^{\xi_L/2}}{1 + a\exp\left(-\frac{180b}{\pi}\arcsin\left(\frac{d_{ud}\sin(\theta_{ud})}{(L^2 + d_{ud}^2 - 2d_{ud}L\cos(\theta_{ud}))^{1/2}}\right) + ab\right)}. \end{aligned} \tag{6}$$

In our work, we take the throughput to measure the performance of covert communications. Based on the received SNR at Receiver, the throughput R is given by

$$R = \log_2(1 + \gamma_r) = \log_2\left(1 + \frac{P f(d_{ud}, \theta_{ud})}{\sigma_r^2}\right). \tag{7}$$

In order to fully utilize the limited energy resources of the UAV for the energy-efficient covert communication, we use covert energy efficiency $\eta\left(P, d_{ud}, \theta_{ud}\right)$ as a measure characterized by the number of bits that can be transmitted per unit energy. Therefore, $\eta\left(P, d_{ud}, \theta_{ud}\right)$ is defined as the ratio between throughput (in bits/s) and communication power consumption (in Watt), which is given by

$$\eta\left(P, d_{ud}, \theta_{ud}\right)=\frac{R}{P}=\frac{1}{P}\log_2\left(1+\frac{Pf\left(d_{ud}, \theta_{ud}\right)}{\sigma_r^2}\right). \quad (8)$$

Actually, the covert energy efficiency as an evaluation metric is a trade-off between transmission performance and energy consumption to depict the throughput per unit energy.

IV. Detection Performance Analysis of Detector

In this section, we analyze the detection performance of Detector and the related minimum detection error probability under noise uncertainty. To realize covert communication, we provide the covertness constraint to ensure that Detector has a high detection error probability for the transmission.

A. Signal Received by Detector

We consider both LoS and NLoS components in the UAV-to-Detector channel to model scenarios where the UAV attempts to conceal itself from Detector. Therefore, $y_d\left[i\right]$ is the received signal at Detector, which is given by

$$y_d\left[i\right]=\begin{cases} n_d\left[i\right], & \mathcal{H}_0, \\ \sqrt{P_d}x\left[i\right]+n_d\left[i\right], & \mathcal{H}_1, \end{cases} \quad (9)$$

where $P_d=Pd_{ud}^{\xi_L}p_d+Pd_{ud}^{\xi_N}(1-p_d)$ is the effective power received at Detector when the UAV transmits, and $n_d\left[i\right]\sim\mathcal{CN}(0,\sigma_d^2)$ is the complex Gaussian noise at Detector. In fact, it is difficult for transceivers to accurately obtain background noise power because of dynamic environmental variations and measurement errors. Therefore, we consider a widely used bounded noise uncertainty model [8], [36], where Detector's noise power σ_d^2 obeys a log-uniform distribution with the following probability density function (PDF)

$$f_{\sigma_d^2}\left(x\right)=\begin{cases} \frac{1}{2\ln(\alpha)x}, & \text{if}\,\frac{1}{\alpha}\widehat{\sigma}_d^2\leq x\leq\alpha\widehat{\sigma}_d^2, \\ 0, & \text{otherwise}, \end{cases} \quad (10)$$

where α denotes the noise uncertainty, and $\widehat{\sigma}_d^2$ is the nominal noise power.

B. Detector's Detection Strategy

Detector performs energy detection to decide the existence of covert transmission, based on its average received power. Detector's detection strategy is given by

$$T_d=\frac{1}{n}\sum_{i=1}^{n}\left|y_d[i]\right|^2\underset{\mathcal{D}_0}{\overset{\mathcal{D}_1}{\gtrless}}\lambda. \quad (11)$$

Here, T_d represents the average value of the received power at Detector, and λ represents the decision threshold. $\mathcal{D}_1$ and $\mathcal{D}_0$ represent the binary decision of whether the UAV is transmitting or not, respectively. We consider that Detector is allowed to observe an infinite number of samples, i.e., $n\to\infty$, which implies that Detector uses a sufficiently long observation window. According to the law of large numbers, Detector's average received power converges to its true expected value, eliminating statistical uncertainty. This represents the worst-case scenario where Detector has maximum detection capability. Consequently, the average received power of Detector is given by

$$T_d=\begin{cases} \sigma_d^2, & \mathcal{H}_0, \\ P_d+\sigma_d^2, & \mathcal{H}_1. \end{cases} \quad (12)$$

The detection error probability is used to measure Detector's detection performance, which is expressed as

$$\begin{aligned} \xi&=P_{\mathrm{FA}}+P_{\mathrm{MD}}=\Pr\left\{\mathcal{D}_1\left|\mathcal{H}_0\right.\right\}+\Pr\left\{\mathcal{D}_0\left|\mathcal{H}_1\right.\right\} \\ &=\Pr\left\{\sigma_d^2\geq\lambda\right\}+\Pr\left\{P_d+\sigma_d^2\leq\lambda\right\} \\ &=1-\Pr\left\{\lambda-P_d<\sigma_d^2<\lambda\right\}, \end{aligned} \quad (13)$$

where the false alarm probability $P_{\mathrm{FA}}=\Pr\left\{\mathcal{D}_1\left|\mathcal{H}_0\right.\right\}$ is the probability that $\mathcal{H}_0$ is true but Detector decides $\mathcal{D}_1$. $P_{\mathrm{MD}}=\Pr\left\{\mathcal{D}_0\left|\mathcal{H}_1\right.\right\}$ is the missed detection probability that $\mathcal{H}_1$ is true but Detector decides $\mathcal{D}_0$.

C. Detector's Minimum Detection Error Probability

We minimize the detection error probability under the worst-case scenario, where Detector optimally adjusts its decision threshold for maximum detection performance. To this end, we adopt a pessimistic assumption that Detector selects the threshold minimizing the detection error probability. Thus, we further consider Detector's minimum detection error probability to assess the covertness of the communication.

Based on the PDF of σ_d^2 as in (10), it can be noted that $\xi=1$ when $\lambda<\hat{\sigma}_d^2/\alpha$, and ξ increases as λ increases when $\lambda>\alpha\hat{\sigma}_d^2$. Therefore, the optimal threshold for minimizing the detection error probability must be in the region $\hat{\sigma}_d^2/\alpha\leq\lambda\leq\alpha\hat{\sigma}_d^2$. For $\hat{\sigma}_d^2/\alpha\leq\lambda\leq\alpha\hat{\sigma}_d^2$, the detection error probability ξ is rewritten as

$$\begin{aligned} \xi&=\begin{cases} 1-\int_{\frac{\hat{\sigma}_d^2}{\alpha}}^{\lambda}f_{\sigma_d^2}(x)dx, & \lambda-P_d\leq\frac{\hat{\sigma}_d^2}{\alpha}, \\ 1-\int_{\lambda-P_d}^{\lambda}f_{\sigma_d^2}(x)dx, & \lambda-P_d>\frac{\hat{\sigma}_d^2}{\alpha}, \end{cases} \\ &=\begin{cases} 1-\frac{1}{2\ln\alpha}\ln\left(\frac{\alpha\lambda}{\hat{\sigma}_d^2}\right), & \lambda\leq P_d+\frac{\hat{\sigma}_d^2}{\alpha}, \\ 1-\frac{1}{2\ln\alpha}\ln\left(\frac{\lambda}{\lambda-P_d}\right), & \lambda>P_d+\frac{\hat{\sigma}_d^2}{\alpha}. \end{cases} \end{aligned} \quad (14)$$

Then, we derive the first-order derivative of the detection error probability ξ relative to the threshold λ as

$$\frac{\partial\xi}{\partial\lambda}=\begin{cases} -\frac{1}{2\ln(\alpha)\lambda}, & \lambda\leq P_d+\frac{\hat{\sigma}_d^2}{\alpha}, \\ \frac{P_d}{2\ln(\alpha)\lambda(\lambda-P_d)}, & \lambda>P_d+\frac{\hat{\sigma}_d^2}{\alpha}. \end{cases} \quad (15)$$

If $\lambda\leq P_d+\hat{\sigma}_d^2/\alpha$, we have $\partial\xi/\partial\lambda<0$, and if $\lambda>P_d+\hat{\sigma}_d^2/\alpha$, $\partial\xi/\partial\lambda>0$. Therefore, according to the optimal threshold region $\hat{\sigma}_d^2/\alpha\leq\lambda\leq\alpha\hat{\sigma}_d^2$, we can derive the optimal threshold λ^* as

$$\lambda^*=\min\left(P_d+\frac{\hat{\sigma}_d^2}{\alpha},\alpha\hat{\sigma}_d^2\right). \quad (16)$$

We note that if $P_d + \hat{\sigma}_d^2/\alpha > \alpha\hat{\sigma}_d^2$, ξ is zero, which means Detector can detect any communication resulting in covert communications never being realized. Therefore, we ignore this case and determine the optimal threshold $\lambda^* = P_d + \hat{\sigma}_d^2/\alpha$, which is substituted into (14) to obtain the minimum detection error probability $\xi_{\min}$ as

$$\xi_{\min} = 1 - \frac{1}{2\ln\alpha}\ln\left(1 + \frac{\alpha P_d}{\hat{\sigma}_d^2}\right). \tag{17}$$

In covert communication, the communication covertness constraint is given by

$$\xi_{\min} \geq 1 - \epsilon, \tag{18}$$

where ϵ is a small value that denotes the covertness requirement. Note that a smaller ϵ corresponds to a higher requirement of communication covertness.

V. Covert Energy Efficiency Maximization

In this section, we maximize the covert energy efficiency while ensuring QoS. Specifically, we present the optimization problem for maximizing the covert energy efficiency by jointly optimizing the location and transmit power of the UAV with the constraints of covertness requirement, UAV throughput, transmit power and flying location. The optimization problem is formulated as

$$\max_{P, d_{ud}, \theta_{ud}} \ \eta\left(P, d_{ud}, \theta_{ud}\right), \tag{19a}$$

$$\text{s.t. } P \leq P_m, \tag{19b}$$

$$\underline{d}_{ud} \leq d_{ud} \leq \overline{d}_{ud}, \tag{19c}$$

$$\underline{\theta}_{ud} \leq \theta_{ud} \leq \frac{\pi}{2}, \tag{19d}$$

$$\xi_{\min} \geq 1 - \epsilon, \tag{19e}$$

$$R \geq R_m. \tag{19f}$$

In the formulation, $\eta\left(P, d_{ud}, \theta_{ud}\right)$ in (19a) as the objective function denotes the covert energy efficiency defined in (8). (19b) is the transmit power constraint and P_m is the maximum transmit power of the UAV. (19c) and (19d) jointly denote the UAV's flying location constraints defined in (1). (19e) is the covertness constraint and ϵ is the covertness requirement. (19f) is the throughput constraint to ensure QoS and R_m represents the minimum throughput requirement for covert communication.

A. Optimal Location Without Constraints

In this subsection, we identify the effect of the UAV's location on covert energy efficiency, which will be used to transform and solve the optimization problem.

Regarding a joint optimization of distance d_{ud} and angle θ_{ud} for maximizing covert energy efficiency $\eta\left(P, d_{ud}, \theta_{ud}\right)$, the UAV's optimal location would be closest to Receiver. Thus, without any constraints, we derive the optimal distance for a given angle and the optimal angle for a given distance.

Following (8), it is clear that covert energy efficiency $\eta\left(P, d_{ud}, \theta_{ud}\right)$ monotonically increases with $f\left(d_{ud}, \theta_{ud}\right)$. Therefore, maximization of $\eta\left(P, d_{ud}, \theta_{ud}\right)$ corresponds to maximizing $f\left(d_{ud}, \theta_{ud}\right)$. The properties of optimal location without constraints are provided in the following lemmas.

Lemma 1: For a given angle θ_{ud}, let $d_{ud}^{\dagger}$ denote the optimal distance between the UAV and Detector that maximizes $\eta(P, d_{ud}, \theta_{ud})$ without constraints. $d_{ud}^{\dagger}$ is the unique solution of the following equation relative to d_{ud}.

$$\frac{\xi_L\left[L\cos\left(\theta_{ud}\right) - d_{ud}\right]}{1 - p_r\left(d_{ud}, \theta_{ud}\right)} = \frac{180bL}{\pi}\sin\left(\theta_{ud}\right), \tag{20}$$

where $p_r\left(d_{ud}, \theta_{ud}\right)$ represents the LoS probability in the UAV-Receiver channel. Then,

$$p_r\left(d_{ud}, \theta_{ud}\right) = \left(1 + a\exp\left[-\frac{180b}{\pi}\arcsin\left(\frac{d_{ud}\sin(\theta_{ud})}{(L^2 + d_{ud}^2 - 2d_{ud}L\cos(\theta_{ud}))^{1/2}}\right) + ab\right]\right)^{-1}. \tag{21}$$

The unique solution to (20) satisfies $d_{ud}^{\dagger} > L\cos\left(\theta_{ud}\right)$. Thus, $\eta\left(P, d_{ud}, \theta_{ud}\right)$ monotonically increases with d_{ud} for $d_{ud} \leq L\cos\left(\theta_{ud}\right)$.

Proof: The first derivative of $f\left(d_{ud}, \theta_{ud}\right)$ relative to d_{ud} can be obtained as

$$\frac{\partial f\left(d_{ud}, \theta_{ud}\right)}{\partial d_{ud}} = \left[L^2 + d_{ud}^2 - 2d_{ud}L\cos\left(\theta_{ud}\right)\right]^{\frac{\xi_L}{2}} \times \left[p_r\left(d_{ud}, \theta_{ud}\right)\frac{\xi_L\left[d_{ud} - L\cos\left(\theta_{ud}\right)\right]}{L^2 + d_{ud}^2 - 2d_{ud}L\cos\left(\theta_{ud}\right)} + \frac{\partial p_r\left(d_{ud}, \theta_{ud}\right)}{\partial d_{ud}}\right], \tag{22}$$

where $p_r\left(d_{ud}, \theta_{ud}\right)$ is given by (21) and the first derivative relative to d_{ud} is derived as

$$\frac{\partial p_r(d_{ud}, \theta_{ud})}{\partial d_{ud}} = \frac{180bL\sin\left(\theta_{ud}\right)p_r(d_{ud}, \theta_{ud})\left[1 - p_r\left(d_{ud}, \theta_{ud}\right)\right]}{\pi\left[L^2 + d_{ud}^2 - 2d_{ud}L\cos\left(\theta_{ud}\right)\right]}, \tag{23}$$

In this scenario, we have $L > d_{ud} > d_{ud}\cos(\theta_{ud})$, $0 < p_r\left(d_{ud}, \theta_{ud}\right) < 1$ and $L^2 + d_{ud}^2 - 2d_{ud}L\cos\left(\theta_{ud}\right) = d_{ur}^2 > 0$. Thus, solving $\partial f\left(d_{ud}, \theta_{ud}\right)/\partial d_{ud} = 0$ is equivalent to solving $F\left(d_{ud}\right) = 0$. Following (22), $F\left(d_{ud}\right)$ is derived as

$$F(d_{ud}) = \xi_L\left[d_{ud} - L\cos(\theta_{ud})\right] + \frac{180bL\sin(\theta_{ud})}{\pi}\left[1 - p_r(d_{ud}, \theta_{ud})\right]. \tag{24}$$

Since $\xi_L < 0$ and $\sin\left(\theta_{ud}\right) > 0$, we obtain $F\left(d_{ud}\right) > 0$ if $d_{ud} \leq L\cos\left(\theta_{ud}\right)$. Then, we further obtain $\partial f\left(d_{ud}, \theta_{ud}\right)/\partial d_{ud} > 0$ for $d_{ud} \leq L\cos\left(\theta_{ud}\right)$. Due to this, we can further obtain the optimal distance $d_{ud}^{\dagger} > L\cos\left(\theta_{ud}\right)$. Moreover, $\partial p_r\left(d_{ud}, \theta_{ud}\right)/\partial d_{ud} > 0$ implies that $F\left(d_{ud}\right)$ monotonically decreases with d_{ud}. Thus, $F\left(d_{ud}\right) = 0$ and its equivalent $\partial f\left(d_{ud}, \theta_{ud}\right)/\partial d_{ud} = 0$ have the same unique solution. We obtain (20) by $F\left(d_{ud}\right) = 0$. ∎

Lemma 2: For a given distance d_{ud}, the optimal flying angle relative to Detector, denoted by $\theta_{ud}^{\dagger}$, that maximizes $\eta(P, d_{ud}, \theta_{ud})$ without constraints can be obtained as the unique solution of the following equation relative to θ_{ud}.

$$\frac{180b}{\pi}\frac{1 - p_r\left(d_{ud}, \theta_{ud}\right)}{L - d_{ud}\cos\left(\theta_{ud}\right)} = \frac{-\xi_L L\sin\left(\theta_{ud}\right)}{\left(L^2 + d_{ud}^2\right)\cos\left(\theta_{ud}\right) - Ld_{ud}\left(1 + \cos^2\left(\theta_{ud}\right)\right)}, \tag{25}$$

where the unique solution to (25) satisfies $\theta_{ud}^{\dagger} < \arccos\left(\frac{d_{ud}}{L}\right)$. Thus, $\eta\left(P, d_{ud}, \theta_{ud}\right)$ monotonically decreases with θ_{ud} for $\theta_{ud} \geq \arccos\left(\frac{d_{ud}}{L}\right)$.

Proof: The first derivative of $f\left(d_{ud}, \theta_{ud}\right)$ relative to θ_{ud} can be obtained as

$$\begin{aligned}&\frac{\partial f\left(d_{ud}, \theta_{ud}\right)}{\partial \theta_{ud}}\\&=\left[p_r(d_{ud}, \theta_{ud})\frac{\xi_L d_{ud} L \sin\left(\theta_{ud}\right)}{L^2+d_{ud}^2-2d_{ud}L\cos\left(\theta_{ud}\right)}+\frac{\partial p_r(d_{ud}, \theta_{ud})}{\partial \theta_{ud}}\right]\\&\quad\times\left[L^2+d_{ud}^2-2d_{ud}L\cos\left(\theta_{ud}\right)\right]^{\frac{\xi_L}{2}},\end{aligned} \tag{26}$$

where $p_r\left(d_{ud}, \theta_{ud}\right)$ is given by (21) and the first derivative relative to θ_{ud} is derived as

$$\begin{aligned}\frac{\partial p_r\left(d_{ud}, \theta_{ud}\right)}{\partial \theta_{ud}}&=p_r\left(d_{ud}, \theta_{ud}\right)\left[1-p_r\left(d_{ud}, \theta_{ud}\right)\right]\frac{180 b d_{ud}}{\pi}\\&\times\frac{\left(L^2+d_{ud}^2\right)\cos\left(\theta_{ud}\right)-d_{ud}L\left[1+\cos^2\left(\theta_{ud}\right)\right]}{\left[L^2+d_{ud}^2-2d_{ud}L\cos\left(\theta_{ud}\right)\right]\left[L-d_{ud}\cos\left(\theta_{ud}\right)\right]}\end{aligned} \tag{27}$$

Since $d_{ud} > 0$, $L^2 + d_{ud}^2 - 2d_{ud}L\cos\left(\theta_{ud}\right) = d_{ur}^2 > 0$, and $0 < p_r\left(d_{ud}, \theta_{ud}\right) < 1$, $\partial f\left(d_{ud}, \theta_{ud}\right)/\partial\theta_{ud} = 0$ is equivalent to $G\left(\theta_{ud}\right) = 0$, where $G\left(\theta_{ud}\right)$ is given by

$$\begin{aligned}G\left(\theta_{ud}\right)=&\frac{180b}{\pi}\frac{\left(L^2+d_{ud}^2\right)\cos\left(\theta_{ud}\right)-Ld_{ud}\left[1+\cos^2\left(\theta_{ud}\right)\right]}{L-d_{ud}\cos\left(\theta_{ud}\right)}\\&\times\left[1-p_r\left(d_{ud}, \theta_{ud}\right)\right]+\xi_L L\sin\left(\theta_{ud}\right).\end{aligned} \tag{28}$$

Here, the term $\left(L^2+d_{ud}^2\right)\cos\left(\theta_{ud}\right)-d_{ud}L\left[1+\cos^2\left(\theta_{ud}\right)\right]$ equals zero when $\theta_{ud} = \arccos\left(\frac{d_{ud}}{L}\right)$. Moreover, we have $L > d_{ud} > d_{ud}\cos\theta_{ud}$, $\xi_L < 0$, and

$$\begin{aligned}&\frac{\partial\left(\left(L^2+d_{ud}^2\right)\cos\left(\theta_{ud}\right)-d_{ud}L\left[1+\cos^2\left(\theta_{ud}\right)\right]\right)}{\partial\theta_{ud}}\\&=\sin\left(\theta_{ud}\right)\left[2d_{ud}L\cos\left(\theta_{ud}\right)-L^2-d_{ud}^2\right]=-\sin\left(\theta_{ud}\right)d_{ur}^2<0.\end{aligned} \tag{29}$$

Thus, we can derive $G\left(\theta_{ud}\right) < 0$ when $\theta_{ud} \geq \arccos\left(\frac{d_{ud}}{L}\right)$, which leads to the conclusion that $\partial f\left(d_{ud}, \theta_{ud}\right)/\partial\theta_{ud} < 0$ for $\theta_{ud} \geq \arccos\left(\frac{d_{ud}}{L}\right)$. Due to this, we can further obtain the optimal angle $\theta_{ud}^{\dagger} < \arccos\left(\frac{d_{ud}}{L}\right)$. In addition, for $\theta_{ud} \geq \arccos\left(\frac{d_{ud}}{L}\right)$, $\partial p_r\left(d_{ud}, \theta_{ud}\right)/\partial\theta_{ud} > 0$, which implies that $p_r\left(d_{ud}, \theta_{ud}\right)$ monotonically increases with θ_{ud}. Furthermore, $\left(L^2+d_{ud}^2\right)\cos\left(\theta_{ud}\right)-d_{ud}L\left[1+\cos^2\left(\theta_{ud}\right)\right]$ and $1/\left[L-d_{ud}\cos\left(\theta_{ud}\right)\right]$ monotonically decrease with θ_{ud}. From (29), $G\left(\theta_{ud}\right)$ decreases monotonically with θ_{ud}. Thus, $G\left(\theta_{ud}\right) = 0$ and $\partial f\left(d_{ud}, \theta_{ud}\right)/\partial\theta_{ud} = 0$ have the same unique solution. We obtain (25) by $G\left(\theta_{ud}\right) = 0$. ■

B. Transformation of the Optimization Problem

In this subsection, we use the trend of covert energy efficiency $\eta\left(P, d_{ud}, \theta_{ud}\right)$ and minimum detection error probability $\xi_{\min}$ relative to location to help transform the optimization problem. To this end, we first identify the trend of $\xi_{\min}$ with P, d_{ud} and θ_{ud} respectively, which is given by the following lemma.

Lemma 3: The minimum detection error probability $\xi_{\min}$ is a monotonic decreasing function of P, a monotonic increasing function of d_{ud}, and a monotonic decreasing function of θ_{ud}.

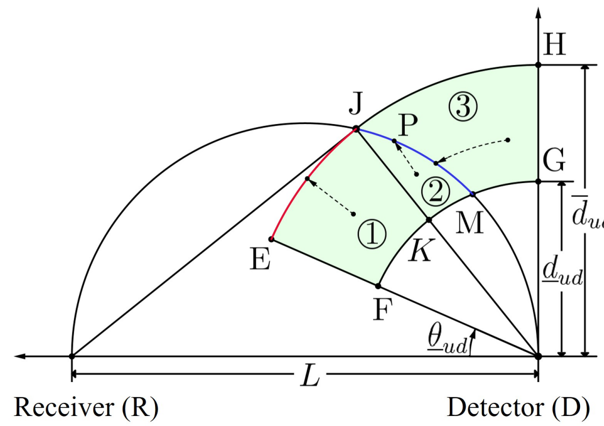

Fig. 2. Schematic of the relative location of the UAV, Detector and Receiver in two-dimensional polar coordinates.

Proof: Based on (17), considering $\xi_{\min}$ as a function of P_d, the first derivative of $\xi_{\min}$ relative to P_d is given by

$$\frac{\partial\xi_{\min}}{\partial P_d} = -\frac{\alpha}{2\ln\left(\alpha\right)\left(\hat{\sigma}_d^2+\alpha P_d\right)}, \tag{30}$$

Considering $\alpha > 1$ and $P_d > 0$, we note that $\partial\xi_{\min}/\partial P_d < 0$, and thus $\xi_{\min}$ monotonically decreases with P_d. In addition, the effective received power at Detector P_d is specifically given by

$$\begin{aligned}P_d &= P d_{ud}^{\xi_L} p_d + P d_{ud}^{\xi_N}\left(1-p_d\right)\\&=\frac{P d_{ud}^{\xi_N}\left(d_{ud}^{\xi_L-\xi_N}-1\right)}{1+a\exp(-180b\theta_{ud}/\pi+ab)}+P d_{ud}^{\xi_N}.\end{aligned} \tag{31}$$

Considering that we have $\xi_N < \xi_L < 0$ and $d_{ud} > 1$ in practice, $d_{ud}^{\xi_L-\xi_N} - 1 > 0$. Therefore, we note that P_d is a monotonic increasing function of P, is a monotonic decreasing function of d_{ud}, and is a monotonic increasing function of θ_{ud}. Due to these, we can conclude that $\xi_{\min}$ is a monotonic decreasing function of P, is a monotonic increasing function of d_{ud}, and is a monotonic decreasing function of θ_{ud}. ■

By the above lemmas and drawing on the proof ideas of [21], we can significantly narrow down the UAV's optimal location and transform the optimization problem in Theorem 1.

Theorem 1: The optimal location $(d_{ud}^*, \theta_{ud}^*)$ for the maximum covert energy efficiency (denoted as η^*) is on the arc defined by $d_{ud} = \overline{d}_{ud}$ and $\underline{\theta}_{ud} \leq \theta_{ud} \leq \arccos\left(\frac{\overline{d}_{ud}}{L}\right)$. This means $d_{ud}^* = \overline{d}_{ud}$ and $\underline{\theta}_{ud} \leq \theta_{ud}^* \leq \arccos\left(\frac{\overline{d}_{ud}}{L}\right)$. Therefore, the optimization problem is simplified as

$$\max_{P,\theta_{ud}}\ \eta\left(P, \overline{d}_{ud}, \theta_{ud}\right), \tag{32a}$$

$$\text{s.t. } P \leq P_m, \tag{32b}$$

$$\underline{\theta}_{ud} \leq \theta_{ud} \leq \arccos\left(\frac{\overline{d}_{ud}}{L}\right), \tag{32c}$$

$$\xi_{\min} \geq 1-\epsilon, \tag{32d}$$

$$R \geq R_m. \tag{32e}$$

Proof: The scenario we consider is represented as a two-dimensional polar coordinate schematic in Fig. 2, where the green region is identified by the flying location constraints (19c) and (19d). The semicircle with diameter L is established by the locations of Receiver and Detector, where $\mathrm{JD} = \overline{d}_{ud}$, $\angle\mathrm{RJD} = 90^{\circ}$ and $\angle\mathrm{RDJ} = \arccos\left(\bar{d}_{ud}/L\right)$.

First, over the region ① (i.e. the region EFKJ), it is proven that the optimal point must be located on the red arc EJ. Since the flying angles relative to Detector of the points in this region satisfy $\theta_{ud} \leq \arccos\left(\bar{d}_{ud}/L\right)$, we have $d_{ud} \leq \bar{d}_{ud} \leq L\cos\left(\theta_{ud}\right)$. For fixed θ_{ud} and $d_{ud} \leq L\cos\left(\theta_{ud}\right)$, Lemma 1 and (8) imply that the objective function, i.e., the covert energy efficiency $\eta\left(P, d_{ud}, \theta_{ud}\right)$, monotonically increases with d_{ud}. The throughput $R = \eta\left(P, d_{ud}, \theta_{ud}\right)P$ in constraint (19f) also monotonically increases with d_{ud}. In addition, the minimum detection error probability $\xi_{\min}$ in the constraint (19e) monotonically increases with d_{ud} by Lemma 3. Therefore, considering the constraint (19c) $\underline{d}_{ud} \leq d_{ud} \leq \overline{d}_{ud}$, we can conclude that $\overline{d}_{ud}$ is the optimal d_{ud} for given θ_{ud}, without regard to the transmit power. This implies that the optimal point in this region lies on the red arc EJ.

Next, over the region ② (i.e. the region JKM), we prove that the optimal point must be located on the blue arc JM. For given θ_{ud}, we have $d_{ud} \leq L\cos\left(\theta_{ud}\right) < \bar{d}_{ud}$. This is illustrated by point $\left(L\cos\left(\theta_{ud}\right), \theta_{ud}\right)$, which has a greater distance from Detector compared to the points with the same angle θ_{ud}. Therefore, the same reasoning as the above region leads to the conclusion that $L\cos\left(\theta_{ud}\right)$ is the optimal d_{ud} for given θ_{ud}, which implies that the optimal point in this region lies on the blue arc JM.

Then, over the region ③ (i.e. the region JMGH), we prove that the optimal point must also be located on the blue arc JM. Since the flying angles of the points over this region satisfy $\theta_{ud} \geq \arccos\left(d_{ud}/L\right)$ for fixed d_{ud}, $\eta\left(P, d_{ud}, \theta_{ud}\right)$ and R monotonically decrease with θ_{ud} by Lemma 2. In addition, $\xi_{\min}$ monotonically decreases with θ_{ud} by Lemma 3. Therefore, for a given d_{ud} within the range $\arccos\left(d_{ud}/L\right) \leq \theta_{ud} \leq \pi/2$, the optimal θ_{ud} is $\arccos\left(d_{ud}/L\right)$. This implies that the optimal point in this region also lies on the blue arc JM.

Finally, we prove that the points on the blue arc JM cannot be the optimal points (excluding point J). For $\arccos\left(\bar{d}_{ud}/L\right) \leq \theta_{ud} \leq \arccos\left(\underline{d}_{ud}/L\right)$, the points on the blue arc JM have $d_{ud} = L\cos\left(\theta_{ud}\right) < \bar{d}_{ud}$, but the optimal distance satisfies $d_{ud}^{\dagger} > L\cos\left(\theta_{ud}\right)$ by Lemma 1. Therefore, for a given θ_{ud}, the optimal d_{ud} is $\min\{d_{ud}^{\dagger}, \bar{d}_{ud}\}$, not $L\cos\left(\theta_{ud}\right)$. This leads to the conclusion that the points on the blue arc JM, except point J, cannot be optimal.

In summary, the optimal flying location of the UAV in the green region is on the red arc EJ, i.e., $d_{ud} = \overline{d}_{ud}$ and $\underline{\theta}_{ud} \leq \theta_{ud} \leq \arccos\left(\bar{d}_{ud}/L\right)$. ■

C. Solution of the Optimization Problem

The solution to the optimization problem (32) is given in the following theorem.

Theorem 2: For the covertness requirement ϵ and minimum throughput requirement R_m, we find the optimal transmit power P^* as a function of the optimal angle θ_{ud}^*, which is given by

$$P^* = \frac{(2^{R_m} - 1)\sigma_r^2}{f(\bar{d}_{ud}, \theta_{ud}^*)}. \tag{33}$$

Based on this, the maximum covert energy efficiency η^* can be expressed as a function of θ_{ud}^* as

$$\eta^* = \frac{f(\bar{d}_{ud}, \theta_{ud}^*)R_m}{(2^{R_m} - 1)\sigma_r^2}. \tag{34}$$

Therefore, we derive η^* as a function of θ_{ud}^*.

Proof: We first determine that the covert energy efficiency $\eta\left(P, d_{ud}, \theta_{ud}\right)$ monotonically decreases relative to P by the first derivative as follows:

$$\frac{\partial\eta\left(P, d_{ud}, \theta_{ud}\right)}{\partial P} = \frac{1}{P^2\ln 2}\left[\frac{zP}{1+zP} - \ln(1+zP)\right], \tag{35}$$

where $z = f\left(d_{ud}, \theta_{ud}\right)/\sigma_r^2$. For $zP > 0$, we have

$$\ln(1+zP) = \int_0^{zP}\frac{1}{1+t}dt > \int_0^{zP}\frac{1}{1+zP}dt = \frac{zP}{1+zP}. \tag{36}$$

Therefore, we can derive $\partial\eta\left(P, d_{ud}, \theta_{ud}\right)/\partial P < 0$, which implies that $\eta\left(P, d_{ud}, \theta_{ud}\right)$ monotonically decreases with P.

According to Lemma 3, $\xi_{\min}$ is a monotonic decreasing function of P. The constraint (32d) defines an upper bound of power P^{ϵ}, which is the root of the equation $\xi_{\min}\left(P\right) = 1 - \epsilon$ and is given by

$$P^{\epsilon} = \frac{\hat{\sigma}_d^2(e^{2\epsilon\ln\alpha} - 1)}{\alpha(\bar{d}_{ud}^{-\xi_L}p_d + \bar{d}_{ud}^{-\xi_N}(1-p_d))}. \tag{37}$$

Moreover, R is a monotonic increasing function of P. The constraint (32e) defines a lower bound of power P^r, which is the root of the equation $R\left(P\right) = R_m$ and is given by

$$P^r = \frac{(2^{R_m} - 1)\sigma_r^2}{f(\bar{d}_{ud}, \theta_{ud})}. \tag{38}$$

As such, for given optimal angle θ_{ud}^*, ϵ and R_m, the feasible power range is $[P^r, \min(P^{\epsilon}, P_m)]$. Based on the fact that the objective function $\eta\left(P, d_{ud}, \theta_{ud}\right)$ is a monotonically decreasing function of P, the optimal transmit power P^* is the lower bound of the feasible range, i.e. $P^* = P^r$. Thus, P^* can be denoted in (33), and (34) can be obtained by substituting (33) into (8). ■

Note that, due to the conflicts between the constraints (32b), (32d) and (32e), the optimization problem (32) is not always feasible. This implies the existence of a feasibility condition for the optimization problem (32), i.e., the requirement that the feasible range is not the empty set. For a given θ_{ud}, the feasibility condition is given by

$$P^r \leq \min\left\{P^{\epsilon}, P_m\right\}. \tag{39}$$

To facilitate intuitive understanding, P^r denotes the UAV's required transmit power for the throughput requirement. P^{ϵ} is the maximum transmit power of the UAV satisfying the covertness constraint. P_m denotes the maximum transmit power of the UAV without covertness constraint. Thus, the feasibility condition means that the required transmit power of the UAV is not more than either of the two maximum transmit powers. This condition also reveals the main trade-off, i.e., increasing the throughput requirement usually requires the UAV to use a larger transmit power, while maintaining covertness restricts the transmit power that can be used. When $P^r > \min\{P^\epsilon, P_m\}$, these performance requirements cannot be satisfied simultaneously. Consequently, covert communication cannot be realized, meaning the maximum covert energy efficiency η^* is zero.

Based on the fact that the maximum covert energy efficiency η^* is derived as a function of the optimal angle θ^*_{ud} in Theorem 2, we can perform a vectorized computation on flying angles based on the constraint (32c) to maximize the covert energy efficiency. The algorithm of vectorized computation for covert energy efficiency maximization is shown in Algorithm 1. Through element-wise vector operations on energy efficiency performance and constraints, the algorithm utilizes a parallel computing architecture to evaluate all candidate angles simultaneously. This elegantly avoids the computational overhead of iterative loops, making it highly efficient for real-world UAV deployments.

The proposed scheme transforms the original three-dimensional joint optimization problem for transmit power and two-dimensional location into a one-dimensional search for the flying angle through theoretical derivations. Therefore, compared to the cubic complexity of traditional three-dimensional search, the computational complexity of Algorithm 1 is significantly reduced and is primarily determined by the dimension N of the angle vector, which depends on the search range and step size, i.e., $N = (\arccos(\overline{d}_{ud}/L) - \underline{\theta}_{ud})/\Delta\theta$, where $\Delta\theta$ denotes the search step size. The algorithm requires executing a constant number of elementary algebraic operations on each element of the N-length vector, implying the time complexity is $\mathcal{O}(N)$. Moreover, the algorithm avoids iterative loops by utilizing vectorization, which eliminates the computational overhead of such loops. Consequently, the algorithm requires memory allocation for several N-length vectors, resulting in a space complexity of $\mathcal{O}(N)$. Considering the explicit angle search range specified in (32c), the memory usage remains entirely within the acceptable range of modern UAV computing resources.

It is worth noting that the mathematical depth of the proposed scheme lies in the dimensionality reduction through theoretical derivations, thereby supporting the application of efficient vectorized algorithms. Compared to optimization techniques that require iterative optimization and yield only suboptimal solutions, such as alternating optimization and successive convex approximation, the proposed scheme achieves global optimality, avoids iterative loops, and achieves efficient computation. This offers significant advantages for UAV platforms that demand computational efficiency.

Algorithm 1 Vectorized computation for solving covert energy efficiency maximization problem

Input: Minimum throughput requirement R_m, covertness requirement ϵ, maximum transmit power P_m, maximum distance $\overline{d}_{ud}$, minimum flying angle $\underline{\theta}_{ud}$, and number of search points N.

Output: UAV's optimal location (d^*_{ud}, θ^*_{ud}), optimal transmit power P^*, and maximum covert energy efficiency η^*.

Problem transformation: Reduce the two-dimensional location constraints to the one-dimensional angle constraint and obtain $d^*_{ud} = \overline{d}_{ud}$, thereby transforming optimization problem (19) into (32).

Initialize: According to $\underline{\theta}_{ud} \le \theta_{ud} \le \arccos\left(\overline{d}_{ud}/L\right)$ in (32c), perform vectorization of the angle search to generate the angle vector $\boldsymbol{\theta}_{ud} = [\theta_1, \theta_2, \ldots, \theta_N]^T$.

Compute the power upper bound vector $\mathbf{P}^\epsilon$ via (37).

Compute the power lower bound vector $\mathbf{P}^r$ via (38).

Compute the binary feasibility vector via (39) as $\mathbf{M} = \text{logical}(\mathbf{P}^r \le \min\{\mathbf{P}^\epsilon, P_m\mathbf{1}\})$, where $\mathbf{1}$ is the all-ones vector.

Compute the energy efficiency vector $\tilde{\boldsymbol{\eta}}$ via (34).

Obtain the effective energy efficiency vector $\boldsymbol{\eta} = \mathbf{M} \odot \tilde{\boldsymbol{\eta}}$, where $\odot$ denotes the entrywise product.

Find the maximum covert energy efficiency $\eta^* = \max(\boldsymbol{\eta})$ and the corresponding index $i^* = \arg\max(\boldsymbol{\eta})$.

if $\eta^* > 0$ **then**

  Obtain $\theta^*_{ud} \leftarrow \boldsymbol{\theta}_{ud}[i^*]$, and calculate P^* via (33).

  return η^*, P^*, and (d^*_{ud}, θ^*_{ud}).

else

  return $\eta^* = 0$, meaning covert communication is unachievable.

end if

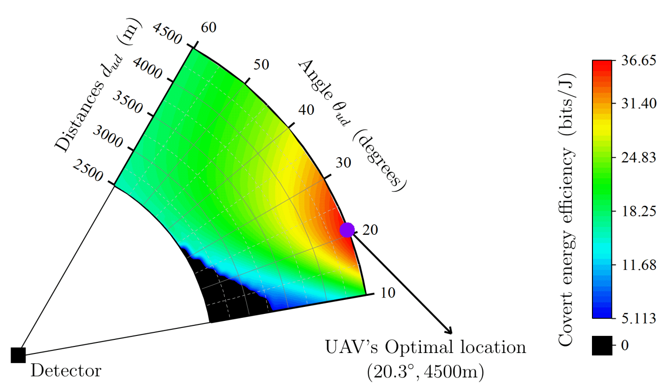

Fig. 3. Heatmap of covert energy efficiency for different flying locations

VI. Numerical Results

In this section, numerical results are provided to illustrate the covert energy efficiency performance with the constraints of covertness, throughput and transmit power. In general, we consider the suburban scenario where the S-curve parameters are given as $a = 4.88$ and $b = 0.429$ [37], and the path loss coefficients for the LoS and NLoS channel components are respectively given as $\xi_L = -2$ and $\xi_N = -3$. If not particularly emphasized, the parameters related to Detector's relative location to UAV and Receiver are given as $L = 10$km and $\underline{\theta}_{ud} = 10°$. The minimum throughput requirement is $R_m = 0.1$bits/s. The UAV's maximum transmit power is $P_m = 10$dBm. The covertness requirement is $\epsilon = 0.04$. The channel parameters are given as $\sigma_r^2 = -60$dBm, $\hat{\sigma}_d^2 = -44$dBm and $\alpha = 6$dB.

Fig. 3 shows a heatmap of covert energy efficiency for different UAV flying locations. Specifically, at certain locations where the feasibility conditions for covert communication

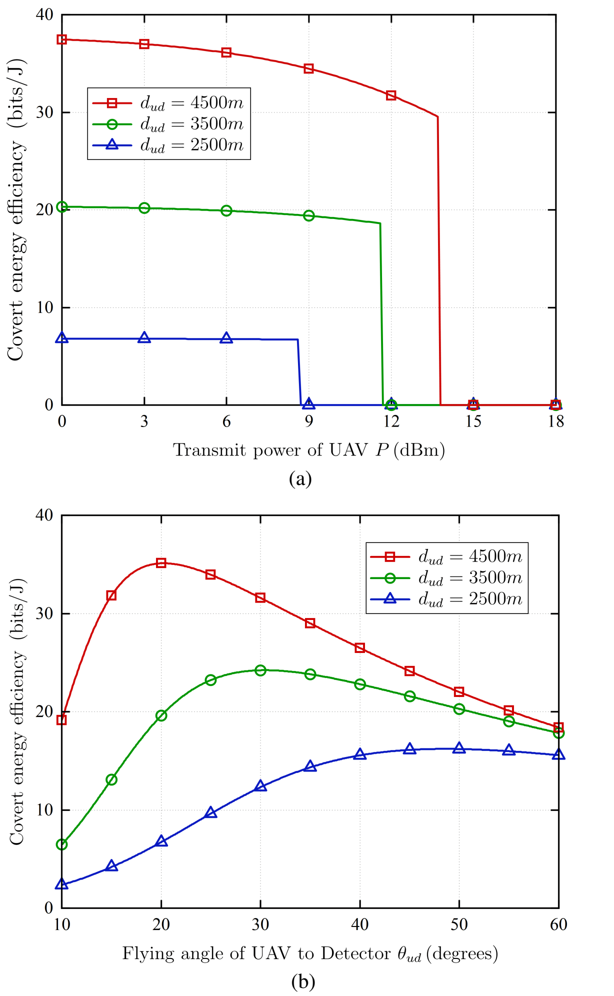

Fig. 4. (a) The covert energy efficiency versus the transmit power of UAV P for the setting of $\theta_{ud} = 30°$. (b) The covert energy efficiency versus the flying angle of the UAV to Detector θ_{ud} for the setting of $P = 8$dBm.

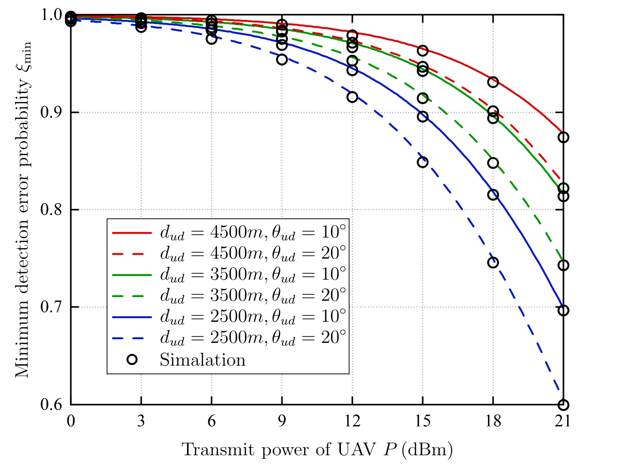

Fig. 5. The minimum detection error probability $\xi_{\min}$ versus the transmit power of UAV P under different UAV locations.

cannot be achieved, the heatmap is colored black, indicating that the covert energy efficiency is zero. For other locations, the magnitude of covert energy efficiency ranges from low to high, corresponding to heatmap colors ranging from blue to red. Additionally, the Detector's location is denoted by a black square, and the UAV's optimal location is marked by a purple circle. It can be observed from Fig. 3 that the UAV's optimal location with the maximum covert energy efficiency is furthest from Detector, which corresponds to the optimal distance being the maximum distance as derived in Theorem 1. The flying angle of the optimal location falls within the feasible range, indicating that a search for the angles is necessary to maximize covert energy efficiency. Furthermore, we can observe that regions with higher covert energy efficiency are generally those farther from Detector and closer to Receiver. This is because these regions can simultaneously ensure relatively better covertness and communication performance. In contrast, the black regions located closer to Detector and farther from Receiver have a covert energy efficiency of zero. This is because, in these regions, the covertness and throughput constraints cannot be satisfied simultaneously, making covert communication unavailable.

Fig. 4 shows the covert energy efficiency versus the transmit power P and flying angle θ_{ud} under different distances d_{ud}. First, we can observe from Fig. 4(a) that, given θ_{ud} and d_{ud}, the energy efficiency decreases and then remains at zero with the increase of P. This is due to the fact that a large P brings a small increase in throughput while costing a large energy consumption. When P increases until the covertness constraint cannot be satisfied, covert energy efficiency remains at zero. From Fig. 4(b), given P and d_{ud}, the covert energy efficiency first increases and then decreases with the increase of θ_{ud}. The reason for this fact is that a larger θ_{ud} makes the angle and distance between the UAV and Receiver larger, which results in the larger path loss and the smaller probability for the LoS channel component between Receiver and UAV. Moreover, in Fig. 4(a) and 4(b), given P and θ_{ud}, we can observe that the energy efficiency increases as d_{ud} increases. This is because the increase in d_{ud} can grant the larger angle and the smaller distance between the UAV and Receiver, which improve the channel gain and the LoS probability, resulting in the larger received power at Receiver. This also indirectly matches the conclusion in Theorem 1 that the optimal d_{ud} is the maximum d_{ud}.

Fig. 5 shows the minimum detection error probability $\xi_{\min}$ versus the transmit power P under different UAV locations. First, we can see that simulated points are consistent with theoretical curves in general, which verifies the correctness of the derivations about $\xi_{\min}$. In the figure, we can observe that, given UAV location, $\xi_{\min}$ decreases with the increase of P. This is due to the fact that the increase of transmit power directly increases the received power at Detector, resulting in the improvement of detection performance and the lower detection error probability. Moreover, given P, $\xi_{\min}$ decreases with the decrease of d_{ud} and decreases with the increase of θ_{ud}. This is because the decrease of d_{ud} or the increase of θ_{ud} can reduce the path loss of the channel between the UAV and Detector, thus improving the received power at Detector and reducing $\xi_{\min}$. All of the above facts correspond to the conclusion in Lemma 3.

Fig. 6 shows the maximum covert energy efficiency η^* of UAV communications versus the covertness requirement ϵ under different maximum distances $\overline{d}_{ud}$. We can see from Fig.

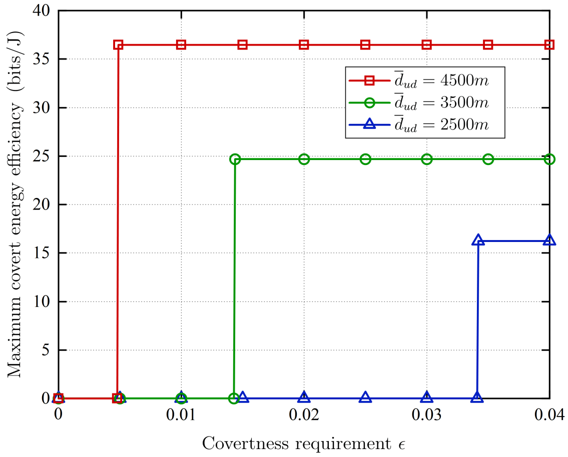

Fig. 6. The maximum covert energy efficiency versus the covertness requirement ϵ under different maximum distances $\overline{d}_{ud}$.

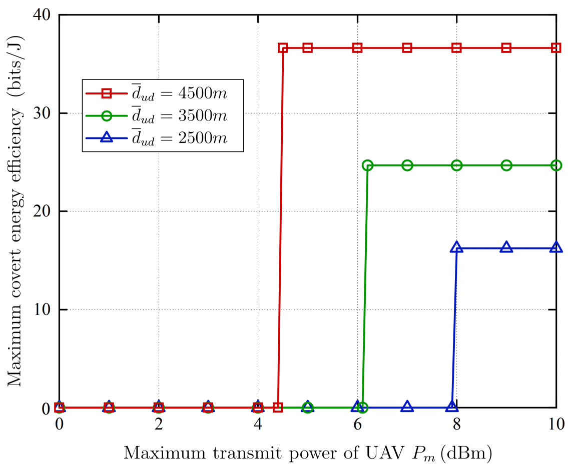

Fig. 7. The maximum covert energy efficiency versus the maximum transmit power P_m under different maximum distances $\overline{d}_{ud}$.

6 that, given $\overline{d}_{ud}$, as ϵ increases, η^* first remains zero, then increases up to a constant and keeps unchanged. The reasons can be explained as follows. When ϵ is small, the covertness constraint is strict, and thus the covertness and throughput constraints cannot be satisfied simultaneously. As a result, η^* equals zero. As ϵ increases until the covertness and other constraints are simultaneously satisfied, η^* remains a constant according to (34) for given R_m. Moreover, given ϵ, η^* increases as $\overline{d}_{ud}$ increases, due to the fact that the large $\overline{d}_{ud}$ increases the objective function and throughput while improving covertness. This also matches Theorem 1.

Fig. 7 shows the maximum covert energy efficiency η^* versus the maximum transmit power P_m under different maximum distances $\overline{d}_{ud}$. We can observe that, given $\overline{d}_{ud}$, η^* first is zero and then increases up to a constant as P_m increases. The reason behind the phenomenon can be explained as follows. When P_m is small, the throughput constraint leads to a lower bound of power, which is greater than P_m. Thus, the throughput constraint cannot be satisfied and η^* is zero. When P_m continues to increase until it is greater than the lower bound, due to the fact that energy efficiency is a decreasing function of power, the optimal power remains at the lower bound. Thus, η^* keeps unchanged. Moreover, as in Fig. 6 identically, η^* increases with $\overline{d}_{ud}$.

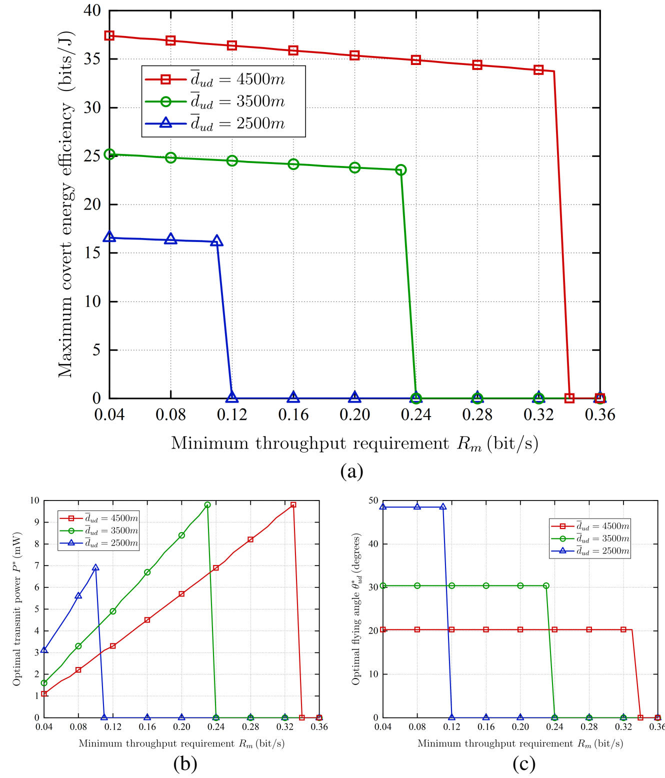

Fig. 8. The maximum covert energy efficiency as well as the corresponding optimal transmit power and flying angle versus the minimum throughput requirement R_m under different maximum distances $\overline{d}_{ud}$.

Fig. 8 shows the maximum covert energy efficiency η^* as well as the corresponding optimal transmit power P^* and flying angle θ^*_{ud} versus the minimum throughput requirement R_m under different maximum distances $\overline{d}_{ud}$. We can observe from Fig. 8(a) that, given $\overline{d}_{ud}$, as R_m increases, η^* first decreases and then keeps zero. The reason is as follows. The covert energy efficiency decreases with transmit power. The larger R_m requires a larger lower bound of power caused by the throughput constraint, which leads to a larger P^*. Thus, η^* first decreases with R_m. When R_m is greater than a threshold value, the throughput constraint cannot be satisfied simultaneously with the covertness or transmit power constraint, resulting in η^* being zero. Accordingly, η^* is determined by P^* and θ^*_{ud}. From Fig. 8(b), P^* first increases until P_m and then becomes unavailable for $\overline{d}_{ud} = \{3500, 4500\}$, while P^* first increases until a lesser value than P_m for $\overline{d}_{ud} = 2500$. This is because when $\overline{d}_{ud}$ is small, the upper bound of power from the covertness constraint (P^{ϵ}) exceeds that of the transmit power constraint (P_m). Moreover, we also note from Fig. 8(c) that, given $\overline{d}_{ud}$, θ^*_{ud} first keeps at a constant and then becomes unavailable. This is due to the fact that changes in angle have a small effect on the covertness, while changes in transmit power can significantly affect covertness and throughput. These properties are illustrated in Fig. 5, and imply that our proposed optimization problem depends mainly on the optimal transmit power. This indicates that there exists an optimal flying location in the current scenario.

To evaluate the performance gain of our scheme, we introduce three benchmark schemes to compare with the

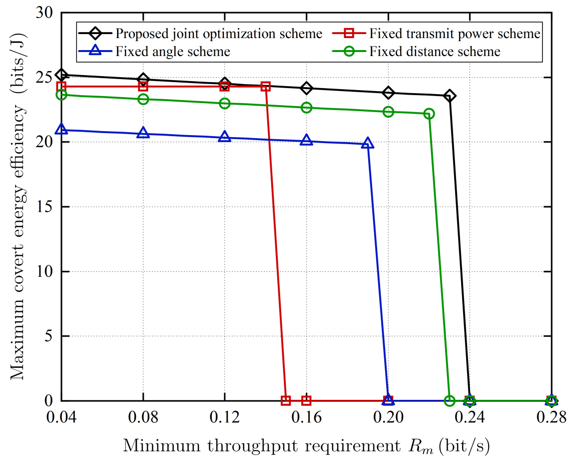

Fig. 9. The maximum covert energy efficiency η^* versus the minimum throughput requirement R_m with different schemes for setting maximum distances $\bar{d}_{ud} = 3500$m.

joint optimization scheme, as shown in Fig. 9. The first of three schemes is the fixed transmit power scheme with $P = 7.8$dBm, the second is the fixed angle scheme with $\theta_{ud} = 40°$, and the third is the fixed distance scheme with $d_{ud} = 3000$m. It can be observed from Fig. 9 that, as the minimum throughput requirement R_m increases, the maximum covert energy efficiency η^* first decreases and then remains at zero for the proposed joint optimization, fixed angle, and fixed distance schemes. This is because the stricter throughput constraint limits the covert energy efficiency, and when it cannot be satisfied simultaneously with other constraints, the covert energy efficiency is zero. For the fixed transmit power scheme, η^* first remains constant and then remains at zero. This is because, for the fixed UAV's transmit power, the UAV's optimal location for maximum energy efficiency is also fixed, causing η^* to remain constant until R_m exceeds a certain threshold. It is important to note that, compared to the benchmark schemes, the proposed joint optimization scheme has a larger η^* and sustains feasibility up to a larger R_m. This implies that the proposed joint optimization scheme offers better energy efficiency performance and can support higher throughput requirements than those schemes with fixed system parameters. Therefore, this result highlights the necessity of joint optimization and shows that proper system parameter setting can enhance system performance.

VII. Conclusion

In this paper, we investigated covert energy efficiency maximization by jointly optimizing UAV transmit power and flying location with the constraints of covertness requirement and UAV covert throughput. We explored the varying properties of energy efficiency, throughput and minimum detection error probability relative to UAV transmit power and flying location. Based on these, we simplified the optimization problem and derived the maximum covert energy efficiency as a function of the optimal flying angle. Then, we maximized covert energy efficiency by searching for flying angles. Through numerical results, we showed that there exists an optimal flying location. Moreover, we found that covertness requirement and maximum transmit power mainly determine whether energy-efficient UAV covert communication is achieved. The minimum throughput requirement not only determines achievement of covert communications, but also affects covert energy efficiency.

References

[1] U. Shafi, R. Mumtaz, N. Iqbal, S. M. H. Zaidi, S. A. R. Zaidi, I. Hussain, and Z. Mahmood, "A multi-modal approach for crop health mapping using low altitude remote sensing, Internet of Things (IoT) and machine learning," *IEEE Access*, vol. 8, pp. 112 708–112 724, 2020.

[2] N. H. Motlagh, T. Taleb, and O. Arouk, "Low-altitude unmanned aerial vehicles-based Internet of Things services: Comprehensive survey and future perspectives," *IEEE Internet Things J.*, vol. 3, no. 6, pp. 899–922, Dec. 2016.

[3] K. P. Valavanis and G. J. Vachtsevanos, *Handbook of unmanned aerial vehicles*. Springer, 2014.

[4] D. He, S. Chan, and M. Guizani, "Communication security of unmanned aerial vehicles," *IEEE Wireless Commun.*, vol. 24, no. 4, pp. 134–139, Aug. 2017.

[5] Y. Zou, J. Zhu, X. Wang, and L. Hanzo, "A survey on wireless security: Technical challenges, recent advances, and future trends," *Proc. IEEE*, vol. 104, no. 9, pp. 1727–1765, Sep. 2016.

[6] B. A. Bash, D. Goeckel, and D. Towsley, "Limits of reliable communication with low probability of detection on AWGN channels," *IEEE J. Sel. Areas Commun.*, vol. 31, no. 9, pp. 1921–1930, Sep. 2013.

[7] I. Makhdoom, M. Abolhasan, and J. Lipman, "A comprehensive survey of covert communication techniques, limitations and future challenges," *Comput. Secur.*, vol. 120, p. 102784, 2022.

[8] B. He, S. Yan, X. Zhou, and V. K. Lau, "On covert communication with noise uncertainty," *IEEE Commun. Lett.*, vol. 21, no. 4, pp. 941–944, Apr. 2017.

[9] J. Hu, S. Yan, X. Zhou, F. Shu, and J. Wang, "Covert communications without channel state information at receiver in IoT systems," *IEEE Internet Things J.*, vol. 7, no. 11, pp. 11 103–11 114, Nov. 2020.

[10] Y. Jiang, L. Wang, and H.-H. Chen, "Covert communications in D2D underlaying cellular networks with antenna array assisted artificial noise transmission," *IEEE Trans. Veh. Technol.*, vol. 69, no. 3, pp. 2980–2992, Mar. 2020.

[11] M. Forouzesh, P. Azmi, N. Mokari, and D. Goeckel, "Covert communication using null space and 3D beamforming: Uncertainty of Willie's location information," *IEEE Trans. Veh. Technol.*, vol. 69, no. 8, pp. 8568–8576, Aug. 2020.

[12] J. Zhang, M. Li, S. Yan, C. Liu, X. Chen, M.-J. Zhao, and P. Whiting, "Joint beam training and data transmission design for covert millimeter-wave communication," *IEEE Trans. Inf. Forensics Security*, vol. 16, pp. 2232–2245, 2021.

[13] J. Hu, S. Yan, X. Zhou, F. Shu, and J. Li, "Covert wireless communications with channel inversion power control in Rayleigh fading," *IEEE Trans. Veh. Technol.*, vol. 68, no. 12, pp. 12 135–12 149, Dec. 2019.

[14] Y. Wu, S. Wang, J. Luo, and W. Chen, "Passive covert communications based on reconfigurable intelligent surface," *IEEE Wireless Commun. Lett.*, vol. 11, no. 11, pp. 2445–2449, Nov. 2022.

[15] Z. Li, X. Liao, J. Shi, L. Li, and P. Xiao, "MD-GAN-Based UAV trajectory and power optimization for cognitive covert communications," *IEEE Internet Things J.*, vol. 9, no. 12, pp. 10 187–10 199, Jun. 2022.

[16] Y. Yang, B. Yang, S. Shen, Y. She, and T. Taleb, "Covert rate study for full-duplex D2D communications underlaid cellular networks," *IEEE Internet Things J.*, vol. 10, no. 17, pp. 15 223–15 237, Sep. 2023.

[17] M. Forouzesh, P. Azmi, A. Kuhestani, and P. L. Yeoh, "Covert communication and secure transmission over untrusted relaying networks in the presence of multiple wardens," *IEEE Trans. Commun.*, vol. 68, no. 6, pp. 3737–3749, Jun. 2020.

[18] X. Li, M. Liu, S. Dang, N. C. Luong, C. Yuen, A. Nallanathan, and D. Niyato, "Covert communications with enhanced physical layer security in RIS-assisted cooperative networks," *IEEE Trans. Wireless Commun.*, vol. 24, no. 7, pp. 5605–5619, Jul. 2025.

[19] X. Li, Z. Tian, W. He, G. Chen, M. C. Gursoy, S. Mumtaz, and A. Nallanathan, "Covert communication of STAR-RIS aided NOMA networks," *IEEE Trans. Veh. Technol.*, vol. 73, no. 6, pp. 9055–9060, Jun. 2024.

[20] Y. Huang, Y. Hu, X. Yuan, and A. Schmeink, "Analytical optimal joint resource allocation and continuous trajectory design for UAV-Assisted covert communications," *IEEE Trans. Wireless Commun.*, vol. 24, no. 1, pp. 213–227, Jan. 2025.

[21] S. Yan, S. V. Hanly, and I. B. Collings, “Optimal transmit power and flying location for UAV covert wireless communications,” *IEEE J. Sel. Areas Commun.*, vol. 39, no. 11, pp. 3321–3333, Nov. 2021.

[22] D. Deng, S. Dang, X. Li, D. W. K. Ng, and A. Nallanathan, “Joint optimization for covert communications in UAV-assisted NOMA networks,” *IEEE Trans. Veh. Technol.*, vol. 73, no. 1, pp. 1012–1026, Jan. 2024.

[23] D. Deng, W. Zhou, X. Li, D. B. da Costa, D. W. K. Ng, and A. Nallanathan, “Joint beamforming and UAV trajectory optimization for covert communications in ISAC networks,” *IEEE Trans. Wireless Commun.*, vol. 24, no. 2, pp. 1016–1030, Feb. 2025.

[24] X. Wu, L. Xu, N. Zhao, X. Jiang, B. Li, W. Lu, and A. Nallanathan, “Covert ambient backscatter communication under surveillance of UAV relaying,” *IEEE Trans. Commun.*, vol. 73, no. 10, pp. 8734–8746, Oct. 2025.

[25] J. Li, D. Wu, C. Yue, Y. Yang, M. Wang, and F. Yuan, “Energy-efficient transmit probability-power control for covert D2D communications with age of information constraints,” *IEEE Trans. Veh. Technol.*, vol. 71, no. 9, pp. 9690–9704, Sep. 2022.

[26] Y. Jiang, Y. Wang, H. Wu, Y. Liu, and L. Hu, “Energy-efficient covert offloading in blockchain-enabled IoT: Joint artificial noise and computation resource allocation,” *IEEE Internet Things J.*, vol. 12, no. 6, pp. 6889–6901, Mar. 2025.

[27] Y. Wang, S. Yan, W. Yang, Y. Huang, and C. Liu, “Energy-efficient covert communications for bistatic backscatter systems,” *IEEE Trans. Veh. Technol.*, vol. 70, no. 3, pp. 2906–2911, Mar. 2021.

[28] J. Chen, J. Wang, Z. Wei, Y. Ren, C. Masouros, and Z. Han, “Joint autonomous underwater vehicle trajectory and energy optimization for underwater covert communications,” *IEEE Trans. Commun.*, vol. 72, no. 11, pp. 7327–7341, Nov. 2024.

[29] D. Deng, X. Li, S. Dang, D. Wing Kwan Ng, A. Nallanathan, and D. Niyato, “Energy efficiency optimization for robust covert ISAC systems,” *IEEE J. Sel. Areas Commun.*, vol. 44, pp. 562–577, Sep. 2025.

[30] X. Sun, W. Tian, M. Du, G. Liu, L. Yang, C. Yuen, and M. Debbah, “Energy-efficient power control and jamming selection falsification for age-aware covert vehicular communications,” *IEEE Internet Things J.*, vol. 13, no. 4, pp. 7152–7166, Feb. 2026.

[31] Y. Wang, S. Yan, X. Zhou, Y. Huang, and D. W. K. Ng, “Covert communication with energy replenishment constraints in UAV networks,” *IEEE Trans. Veh. Technol.*, vol. 71, no. 9, pp. 10 143–10 148, Sep. 2022.

[32] Y. Zhou, A. Al-nahari, R. Jäntti, Z. Ma, and P. Fan, “Energy-efficient covert communications for UAV-assisted backscatter systems,” *IEEE Trans. Veh. Technol.*, vol. 73, no. 6, pp. 9147–9152, Jun. 2024.

[33] X. Zhou, S. Yan, D. W. K. Ng, and R. Schober, “Three-dimensional placement and transmit power design for UAV covert communications,” *IEEE Trans. Veh. Technol.*, vol. 70, no. 12, pp. 13 424–13 429, Dec. 2021.

[34] D. Wang, X. Zhao, W. Shen, Z. Li, N. Cheng, H. Qin, and L. Cao, “Optimal transmit power and hovering location for UAV covert communication in IoT systems,” *IEEE Internet Things J.*, vol. 11, no. 15, pp. 26 118–26 130, Aug. 2024.

[35] A. Al-Hourani, S. Kandeepan, and S. Lardner, “Optimal LAP altitude for maximum coverage,” *IEEE Wireless Commun. Lett.*, vol. 3, no. 6, pp. 569–572, Dec. 2014.

[36] X. Zhou, S. Yan, J. Hu, J. Sun, J. Li, and F. Shu, “Joint optimization of a UAV’s trajectory and transmit power for covert communications,” *IEEE Trans. Signal Process.*, vol. 67, no. 16, pp. 4276–4290, Aug. 2019.

[37] J. Holis and P. Pechac, “Elevation dependent shadowing model for mobile communications via high altitude platforms in built-up areas,” *IEEE Trans. Antennas Propag.*, vol. 56, no. 4, pp. 1078–1084, Apr. 2008.

Yangfan Xu received the B.S. degree from Huazhong Agricultural University in 2022. He is currently pursuing a M.S. degree in computer technology at Anhui University. His research interest focuses on the covert communication in the physical layer.

Bin Yang received his Ph.D. degree in systems information science from Future University Hakodate, Japan in 2015. He was a research fellow with the School of Electrical Engineering, Aalto University, Finland, from Nov. 2019 to Nov. 2021. He is currently a professor with the School of Computer and Information Engineering, Chuzhou University, China. His research interests include unmanned aerial vehicle networks, cyber security and Internet of Things.

Yulong Shen received the B.S. and M.S. degrees in computer science and the Ph.D. degree in cryptography from Xidian University, Xi’an, China, in 2002, 2005, and 2008, respectively. He is currently a Professor with the School of Computer Science and Technology, Xidian University, where he is the Associate Director of the Shaanxi Key Laboratory of Network and System Security and a member of the State Key Laboratory of Integrated Services Networks. His research interests include wireless network security and cloud computing security. He has served on the technical program committees of several international conferences, including ICEBE, INCoS, CIS, and SOWN.

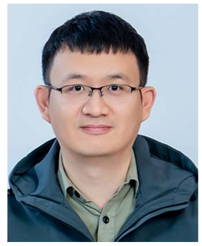

Zhiquan Liu received the BS degree from the School of Science, Xidian University, Xi’an, China, in 2012, and the PhD degree from the School of Computer Science and Technology, Xidian University, Xi’an, China, in 2017. He is currently a full professor, doctoral supervisor, and deputy dean with the College of Cyber Security, Jinan University, Guangzhou, China. His current research focuses on security, trust, privacy, and intelligence in vehicular networks and UAV networks. He currently serves as the area editor or associate editor of multiple SCI-index journals, such as IEEE Transactions on Information Forensics and Security, IEEE Transactions on Dependable and Secure Computing, IEEE Transactions on Industrial Informatics, IEEE Transactions on Vehicular Technology, IEEE Internet of Things Journal, IEEE Network, Information Fusion, etc. His homepage is https://www.zqliu.com.

Xiaohong Jiang received the B.S., M.S., and Ph.D. degrees from Xidian University, China, in 1989, 1992, and 1999, respectively. From February 2005 to March 2010, he was an Associate Professor with Tohoku University. He is currently a Full Professor with Future University Hakodate, Japan. He has published over 300 technical articles at premium international journals andconferences, which include over 80 articles published in top IEEE journals and top IEEE conferences, such as the IEEE/ACM TRANSACTIONS ON NETWORKING(TON), the IEEE JOURNAL OF SELECTED AREAS ON COMMUNICATIONS (JSAC), and the IEEE International Conference on Computer Communications (IEEE INFOCOM). His research interests include wireless networks, network security, optical networks, and router/switch design.

Tarik Taleb received the B.E. degree with distinction in Information Engineering and the M.Sc. and Ph.D. degrees in Information Sciences from Tohoku University, Sendai, Japan, in 2001, 2003, and 2005, respectively. He is currently a Full Professor at Ruhr University Bochum (RUB), Germany, where he leads research activities on next-generation mobile and distributed systems. Prior to joining RUB, he was a Professor at the University of Oulu, Finland (2018–2023), and an Associate Professor at Aalto University, Finland (2014–2021). Earlier in his career, he served as a Senior Researcher and 3GPP Standards Expert at NEC Europe Ltd., Heidelberg, Germany, where he contributed to the evolution of mobile network architectures and standardization activities. Before joining NEC, he was an Assistant Professor at the Graduate School of Information Sciences, Tohoku University, Japan, working in a research laboratory fully funded by KDDI. He also held a Research Fellowship at the Intelligent Cosmos Research Institute, Japan, from 2005 to 2006. Prof. Taleb is widely recognized for his pioneering contributions to mobile network softwarization, network slicing, cloud-edge continuum management, and autonomous networking. His current research interests include autonomous network and service management, edge-cloud continuum systems, network softwarization and slicing, software-defined security, and AI-native communication networks.